THE JOURNAL OF PHYSICAL CHEMISTRY C

Article

Cite This: J. Phys. Chem. C 2019, 123, 4755−4766

pubs.acs.org/JPCC

Effective Interactions between Calcium-Silicate-Hydrate Nanolayers

Saeed Masoumi,[†] Siavash Zare,[‡] Hamid Valipour,[†] and Mohammad Javad Abdolhosseini Qomi*[,‡]

[†]Centre for Infrastructure Engineering and Safety (CIES), School of Civil and Environmental Engineering, UNSW Australia, UNSW, Sydney, NSW 2052, Australia

[‡]Advanced Infrastructure Materials for Sustainability Laboratory (AIMS Lab), Department of Civil and Environmental Engineering, Henry Samueli School of Engineering, E4130 Engineering Gateway, University of California, Irvine, Irvine, California 92697-2175, United States

Supporting Information

ABSTRACT: Calcium-silicate-hydrate (C-S-H), the main binding phase in cementitious materials, possesses a complex multiscale porous texture where nanosized particles interact effectively and contribute to the macroscopic properties of concrete. Engineering the morphology and properties of cementitious materials can thus be obtained by, first, studying the impact of the variable chemical composition on the cohesion and properties of nanolayers of C-S-H at the nanoscale and, then, translating these information to the mesoscale so that a textural analysis can be accomplished. Here, we aim to establish a foundation for such a comprehensive study. First, we construct variable atomic structures of C-S-H nanolayers and validate them against experimental measurements. Then, we conduct free energy perturbation analysis to measure the potential-of-mean-force (PMF) between C-S-H nanolayers with varying chemical compositions. We find a strong correlation between the chemical composition as well as polymorphic structure of C-S-H and characteristics of measured PMFs. In particular, we observe a transition in PMF shape from a single minimum to multiple minima, indicating the emergence of metastable states in the interparticle interactions. We show that key mechanical properties of C-S-H calculated via the PMF approach are in a reasonable agreement with the available experimental data. The proposed PMFs can be directly used to investigate the textural attributes as well as the study of the hydration process in cementitious materials.

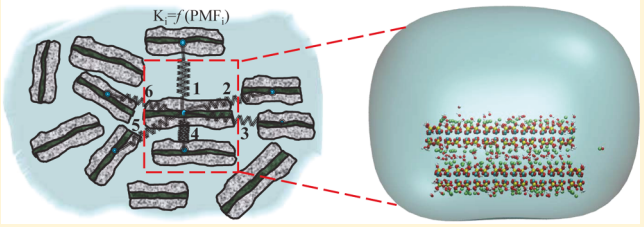

INTRODUCTION

Cementitious materials are ubiquitously used in constructions to glue aggregates and form concrete. The characteristic of the cohesion in cement is attributed to the formation of calcium-silicate-hydrate (C-S-H) gel in a hydration process in which C-S-H globules precipitate from the cement grains.[1] C-S-H globules, as the building blocks of the C-S-H assembly, consist of stacked nanolayers with variable chemical compositions. Consequently, to be able to design and control superior properties of concrete, that is, high strength/volume ratio, it is highly informative to investigate the impact of variable chemical compositions on the effective interactions between C-S-H nanolayers during the hydration process.[2−4] This is more pronounced when one considers the effect of these heterogeneities on the mesotexture of cement hydrates.[5,6]

Despite the recent research efforts, the nanoscale structure of C-S-H still remains enigmatic and subject of intensive research.[7−11] Among existing C-S-H models, defective Tobermorite models are carefully studied and are rather straightforward to construct and tune their stoichiometry.[9] Taylor suggested that the Ca/Si ratio can be adjusted by manipulating silicate chains, that is, removal of silica groups (SiO_2), as well as adding interlayer calcium hydroxyl groups.[12] These defective C-S-H layers agglomerate at the mesoscale to form the so-called nanogranular texture for cement hydrates, as suggested by adsorption,[13] nanoindentation,[14] and small-angle neutron[15−17] and X-ray[18−20] scattering experiments. The aggregation of C-S-H nanolayers is due to the interparticle cohesion and can be studied in the realm of colloidal stability.[21]

The cohesion between charged colloidal particles in a solvent has been the subject of interest in the physical chemistry community for decades, and it is conventionally discussed within the framework of mean-field theories.[22−27] In these approaches, one usually solves the Poisson−Boltzmann equation and works out the distribution of counterions, electrostatic potential, and electric field away from colloids. In these theories, it is assumed that the thermodynamic properties of the electrolyte solution around particles are akin to that of the bulk state. Moreover, the distribution of ions in the interlayer pore is expected to follow the Boltzmann distribution, which limits the application to dilute systems. The pioneering mean-field theory to describe the stability of colloidal systems is the Derjaguin−Landau−Verwey−Overbeek (DLVO) theory.[28,29] In the DLVO framework, the overall interaction between charged colloids is decomposed in two

Received: August 21, 2018
Revised: January 2, 2019
Published: February 7, 2019

DOI: 10.1021/acs.jpcc.8b08146
J. Phys. Chem. C 2019, 123, 4755−4766

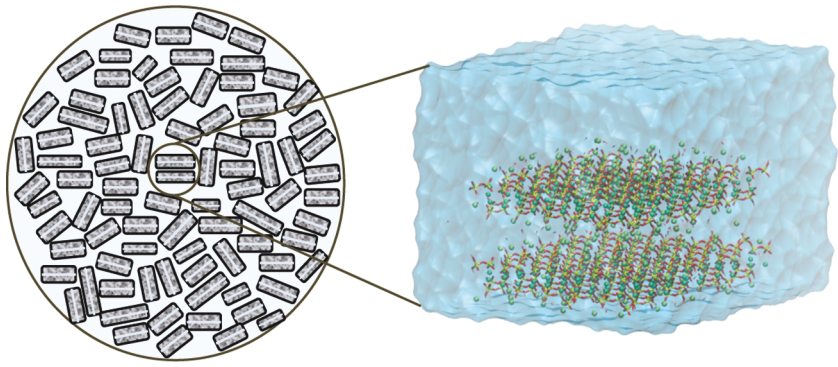

Figure 1. Schematic representation of calcium-silicate-hydrate globules. C-S-H globules interact with their adjacent globules and form a cohesive nanogranular texture that binds constituents in cementitious materials at the macroscale. The strength of the interaction between two nanolayers of C-S-H at short distances can be measured via full atomistic simulation with the emphasis on capturing surface details and local effects. In the zoomed-in window shown on the right, spheres with lime and cyan colors represent interlayer calcium and intralayer calcium atoms, respectively. Furthermore, we illustrate the Si−O bonds as yellow-red and O−H bonds as red-white pipes.

contributions, namely, double-layer repulsive and van der Waals attractive forces. Although the DLVO theory provides a simple and yet powerful tool for measuring the stability of colloidal assemblies, it is formulated for colloidal particles with low surface charge density (SCD) and assumes an ideal gas description for ions. To provide a more effective tool for highly charged colloids, primitive models are proposed, which bear in themselves the simplicity of mean-field calculations while providing more reliable predictions.[21,30,31] In these models, the charges on colloids are considered to be uniformly distributed at the surface, and the solvent is treated as bulk, that is, the dielectric continuum assumption. The interaction between colloids is then due to the competition between entropic repulsive and attractive forces between colloids and counterions. However, the dielectric continuum assumption limits the application of these models at short distances where local effects such as solvation forces,[32,33] structural asperities,[34] and entropic effects are significant.[22]

C-S-H nanoparticles have high surface charge density (SCD),[35] variable surface asperity, and hydrophilic surface attributes[36] depending on their calcium-to-silicon (Ca/Si) ratio. While at large separation distances C-S-H particles can be treated within the continuum framework, at short distances, a more theoretically robust approach is required to resolve strong local effects. This highlights the importance of full atomistic simulations as it portrays atomic-level details and hence is more suitable to investigate the interparticle interactions at short distances.[32,34,37−39]

In this paper, we study the impact of chemical compositions on the effective interactions between the C-S-H nanolayer in aqueous solution. We begin with constructing the atomic structure of finite-sized C-S-H nanolayers at varying Ca/Si ratios. We monitor the protonation of constructed models by allowing chemical reactions between nanolayers and aqueous solution via the reactive molecular dynamics (MD) simulation approach. Having proper structures of finite-sized C-S-H layers at hand, we calculate the dielectric constant of the nanoconfined water in the pore between C-S-H nanolayers and examine the distance range in which full atomistic simulations are indispensable. Subsequently, we measure potential-of-mean-forces (PMFs) between full atomistic C-S-H nanolayers via the free energy perturbation (FEP) method and analyze them in depth to identify the contribution of different groups of atoms to the overall PMF shape. Finally, we summarize our PMF results by providing an analytical interparticle interaction model that can be used in mesoscale simulations of C-S-H gels.

METHODS AND MATERIAL MODELS

In this section, first, we explain general aspects of our simulation setups and then discuss the adjustment of Ca/Si in the C-S-H atomic structure along with the protonation of oxygen atoms and validate our structure against available experimental observations.

Simulation Setups. Here, we use LAMMPS software[40] for molecular dynamics (MD) simulations. Also, throughout this paper, for nonperiodic C-S-H nanolayers (which will be discussed in the next sections), we always use a supercell of 3 × 2 × 1 inside a periodic simulation box with a gap size of 7.5 Å from each side (see Figure 1). After placing the nanolayers inside the simulation box, we saturate the medium with simple point charge water molecules such that the density of water becomes 1 g/cm^3. For periodic nanolayers, we use the periodic supercell of 2 × 2 × 1 inside a saturated simulation box. Moreover, we use CSHFF forcefield[41,42] to define the interatomic interaction in the C-S-H system except from reactive simulations. CSHFF forcefield is based on the partial atomic charges and has been extensively used for cementitious materials.[8,32,34,42−44] In all MD simulations, we keep the temperature at 300 K using a Nosé−Hoover thermostat.[45]

In nonreactive simulations, we treat bonds inside molecules as rigid using the SHAKE algorithm and therefore restraining internal vibration. Furthermore, we freeze vibrations of atoms in the silicate chain backbone. Nevertheless, we let water molecules, hydroxyl groups (either inside the nanolayer or in the solution), and interlayer calcium atoms to move freely during MD simulations. This is because dynamics of atoms inside the nanolayer does not influence the PMF significantly.[32] Owing to the restrictions imposed on species, we choose a time step of 2 fs to capture the dynamics of mobile species.

We use the FEP method to calculate PMF between nanolayers of C-S-H. In FEP, we conduct a series of independent MD simulations at evenly spaced distances along a predefined interaction path. Furthermore, we use uncorrelated simple overlap sampling with forward−backward perturbations to sample important regions of the phase space. Assuming a linear variation in the Hamiltonian of the system,

DOI: 10.1021/acs.jpcc.8b08146
J. Phys. Chem. C 2019, 123, 4755−4766

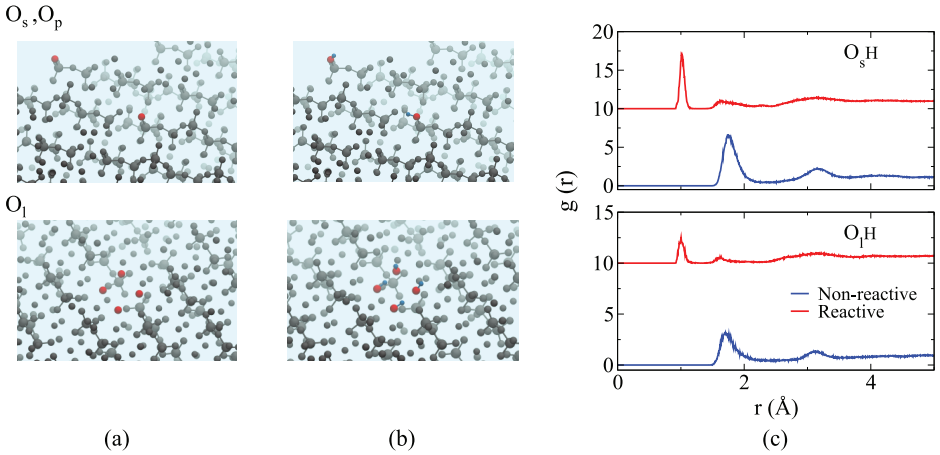

Figure 2. Protonation of oxygen atoms and formation of hydroxyl groups in C-S-H nanolayers. (a) Side (O_s), pairing (O_p), and lone (O_l) oxygen atoms before the reactive simulation setup. Oxygen atoms are identified with a red sphere; (b) oxygen atoms after protonation. Hydrogen atoms that reacted with these oxygen atoms are depicted via blue spheres. Almost all O_s and O_l atoms react with the solution and form hydroxyl groups. (c) Pair correlation functions for O_s−H and O_l−H pairs in the reactive and nonreactive environments. The peak at 1 Å for reactive simulation indicates the formation of O−H bond. For nonreactive simulations, the peak remains at ≈1.65 Å, indicating the tendency of O_s and O_l atoms to attract water hydrogen atoms to balance their negative excess charge.

we calculate Helmholtz free energy in the canonical ensemble as[46]

$$\Delta A_{i,i+1} = -\frac{1}{\beta}\ln\left[\frac{\langle \exp(-\beta \Delta U_{i,i+1}/2)\rangle_i}{\langle \exp(-\beta \Delta U_{i+1,i}/2)\rangle_{i+1}}\right] \quad (1)$$

where A corresponds to the so-called Helmholtz free energy and $\Delta U_{i,i+1}$ is the total potential energy difference between states i + 1 and i.[34] Also, $\beta = 1/k_BT$, where k_B and T are, respectively, the Boltzmann constant and the absolute temperature. We run simulations for 3 ns in the canonical ensemble while sampling the phase space every 2 ps in the last 2 ns. This results in 1000 frames and accordingly 2000 associated perturbations. We choose an interval of 0.125 Å between successive states in all FEP calculations to ensure convergence of FEP calculations.[34]

Stoichiometry of C-S-H Nanolayers. The exact mechanism of how the nanostructure of C-S-H adopts to the variation of Ca/Si is still ambiguous and the subject of intensive research. Here, we follow the mechanism of adjusting the Ca/Si ratio for C-S-H based on the combinatorial approach proposed by Qomi et al.[8]

To begin with, we take the structure of Tobermorite proposed by Hamid (Ca/Si = 1)[47] and tailor its structure to achieve the desired Ca/Si. At its core, Tobermorite $Ca_6[Si_6O_{18}]\cdot 2H_2O$[47] has a Ca−O pseudo-octahedral sheet surrounded by silicate chains, which hold a kinked pattern with repetition periodicity of three tetrahedra (dreierketten pattern[12,48]). Two pairing silicate tetrahedra in the dreierketten pattern are linked together at the same level with respect to the calcium sheets while the bridging silicate tetrahedra protrude away from the surface level of pairing sites (see the Supporting Information for further details). Since the original Hamid's Tobermorite cell has a large tilt angle, we reshape it via a hexagonal-to-orthogonal transformation to simplify working around coordinates.[32] This leads to a unit cell with final lattice parameters of a = 13.2 Å, b = 24.5 Å, c = 12.20 Å, α = 82.5°, β = 90°, γ = 90°. In this paper, unless otherwise stated, we use finite-sized models to enable unconstrained exchange of ions inside the solution and mimic a nanogranular C-S-H structure. We attain this by removing periodic boundary conditions such that silicates are tetrahedrally coordinated. To cope with the dreierketten pattern, we remove chains' ending sites in the case that they are either a bridging silicate tetrahedron or a pairing silicate tetrahedron. In other words, if we assign 1 to a pairing silicate tetrahedron and 2 to a bridging silicate tetrahedron, we make sure that a silica chain starts with 112 and ends with 211.

The next step toward forming C-S-H nanolayers is to customize its Ca/Si ratio. The adjustment of the Ca/Si ratio should necessarily lead to a structure that is consistent with experimental observations. On the one hand, from previous experiments, mean silica chain length (MCL) decreases as the Ca/Si ratio increases from 1 to 1.5.[8,49−51] This can be interpreted as the depolymerization of silicates from nanolayers. On the other hand, increase in Ca/Si can be accompanied by the substitution of interlayer calcium atoms for bridging silicate tetrahedra.[9,52,53] One can increase the Ca/Si ratio either by adding calcium atoms to the interlayer space or by imposing defects, that is, removing silicates from chains. While in this work we follow the combinatorial procedure based on the depolymerization of silicates as outlined by previously,[8] we examine the effect of adding interlayer calcium atoms for the case of Ca/Si = 1.3 as it can be considered as the boundary between the crystalline and disordered structure.[8]

To increase the Ca/Si ratio, we primarily take out bridging silicate tetrahedra atoms. This includes removing a silicon atom together with two nonbridging oxygen atoms attached to it. We commence by eliminating pairing silicate tetrahedra atoms after complete depletion of bridging silicate tetrahedra atoms. For the case where we increase Ca/Si by adding Ca atoms, we place them in the position of absent bridging silicate tetrahedra atoms.

Protonation of C-S-H Nanolayers. In this part, we consider reactions between previously built C-S-H nanolayers and the surrendering aqueous solution. To map out the protonation of nanolayers, we carry out reactive simulations by employing ReaxFF forcefield.[54−56] ReaxFF forcefield takes into account the contribution of chemical bonding into the potential energy via distance-dependent bond order functions. Thus, it captures the formation and breakage of bonds and

DOI: 10.1021/acs.jpcc.8b08146
J. Phys. Chem. C 2019, 123, 4755−4766

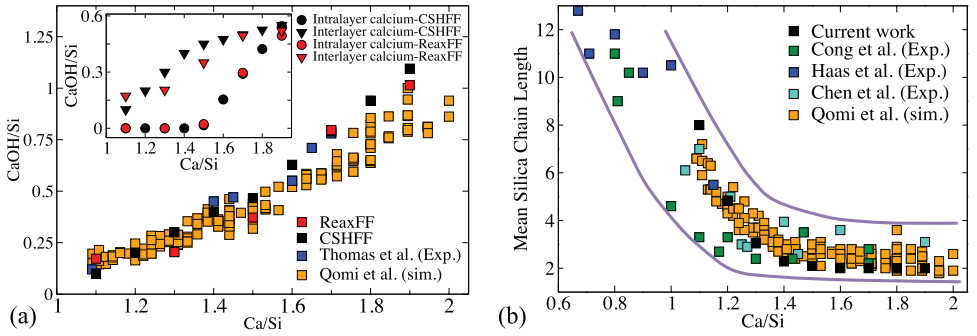

Figure 3. Comparison between the structure of C-S-H models developed in this work and other experimental and simulation results. (a) Ca−OH/Si for different Ca/Si ratios. For Ca/Si < 1.5, only interlayer CaOH/Si is present in the system. The ReaxFF simulations show a sharp increase in the ratio of interlayer CaOH up to Ca/Si = 1.5. For Ca/Si ≥ 1.5, intralayer CaOH/Si contribution emerges and simultaneously the increase in interlayer CaOH/Si becomes constant. After following the trend observed from the reactive environment, we modify the atomic structure of the C-S-H with total CaOH/Si imitating ReaxFF simulations' result automatically. Results are consistent with those reported in the experiments[57] and reactive simulations for infinite C-S-H nanolayers.[8] (b) Mean chain length of C-S-H nanolayers as a function of Ca/Si ratio. Increase in Ca/Si results in the decrease in MCL. Trendlines are a guide for the eye. The result is compared with previous reports from experiments[49−51] and simulations.[8]

suits our purpose to measure the level of nanolayers' protonation.

In ReaxFF simulations, we use finite-sized models in the canonical ensemble and place a nanolayer of C-S-H inside the simulation box. Simulations are performed for 500 ps with the time step of 0.2 fs to properly capture reactions and dynamics of the system. During simulations, we freeze intralayer calcium atoms to prevent artificially large transitional and rotational motion of the C-S-H nanolayer across the simulation box.

For the sake of comparison and clarity, we label oxygen atoms presented in the system based on their local environment. To this end, we name oxygen atoms at the end of silicate chains O_s. Also, we designate ending oxygen atoms that remain attached to a pairing site after depolymerization of bridging silicate sites O_p. Moreover, four oxygen atoms left unpaired after removing a dimer (for Ca/Si ≥ 1.5) are named O_l. Figure 2a,b schematically represents these species before and after protonation.

We calculate radial distribution function (RDF) in reactive and nonreactive environments for O_s−H and O_l−H pairs and report the average over the last 100 ps of simulations as follows

$$\chi_\alpha \chi_\beta \rho g(r) = \langle \frac{1}{N} \sum_{i=1}^{N_\alpha} \sum_{j=1, i\neq j}^{N_\beta} \delta(r - r_j + r_i) \rangle \quad (2)$$

where χ_x and N_x, respectively, denote the molar fraction and the total number of atomtype x. We exclude O_p−H RDF due to its similarity to the O_s−H trend. Also, we run nonreactive MD simulations in the canonical ensemble for 1 ns and calculate RDF in the last 500 ps between selected pairs (see the Methods and Material Models section for details of simulations). As it is evident from Figure 2c for both O_s−H and O_l−H pairs, the peak is located at 1 Å in the reactive environment, whereas for the nonreactive case, it occurs at ≈1.65 Å. This stems from distinct environment settings and the fact that water molecules in reactive simulations have broken down to hydroxyl groups and protons, whereas this capability is absent in classical CSHFF potential. By analyzing MD trajectories, we find that almost all O_s atoms become saturated with protons, whereas O_p atoms show 50% reaction for crystalline C-S-H (Ca/Si < 1.5) and approximately 25% for the glassylike C-S-H (Ca/Si ≥ 1.5). Also, almost all O_l atoms tend to react and form hydroxyl groups within the nanolayer (for further details, see the Supporting Information). Following the observed pattern in reactive simulations, we saturate all O_s and O_l atoms in our models. Furthermore, upon removing a bridging site, we saturate one of two O_p atoms.

As demonstrated in Figure 3, we compare the structure of our models with available experimental data from the literature. From Figure 3a, our ReaxFF calculations show a proportional increase with respect to CaOH/Si versus Ca/Si, which is in a good agreement with inelastic neutron spectroscopy (INS) measurements[57] and ReaxFF simulations of bulk C-S-H.[8,36] Furthermore, we distinguish between the contributions of intralayer and interlayer calcium atoms into the CaOH/Si ratio. While intralayer calcium atoms vibrate inside the nanolayer and are expected to explore a small region during their vibration, interlayer calcium atoms are freely vibrating at the surface level of nanolayers. We see from the inset of Figure 3a that the amount of interlayer CaOH/Si inclines as Ca/Si raises with the sharper trend from 1.1 to 1.5. For Ca/Si ≥ 1.5, as more pairing sites are eliminated from the nanolayer, the contribution of intralayer CaOH/Si emerges and becomes notable for higher Ca/Si. This is due to ionic diffusions into the position of missing silica tetrahedra inside the nanolayer. Following INS observations[57] and reactive simulation trends, we establish an automatic scheme to generate comparable CaOH/Si (see Figure 3a).

Another structural feature of interest is the mean silicate chain length (MCL). Figure 3b shows the trend in which MCL varies with respect to the Ca/Si ratio. While similar MCL does not necessarily guarantee the same surface structure and consequently cannot be a solid evidence for detailed similarities between models and the real C-S-H structure, any proposed C-S-H structure based on experimental observations must have at least similar MCL values obtained from experiments. In our models, MCL decays sharply as Ca/Si increases from 1.1 to 1.5. Owing to the absence of monomers in the system,[58] for Ca/Si > 1.5, MCL becomes two, which stems from the mere presence of dimers in our C-S-H nanolayer. Our scheme leads to an MCL value that is reasonably close to experimental[49−51] and simulation[8] measurements.

Obtaining atomic charges require calculations of electronic charge densities around nuclei within the ab initio framework. This is computationally expensive for C-S-H nanolayers

DOI: 10.1021/acs.jpcc.8b08146
J. Phys. Chem. C 2019, 123, 4755−4766

containing hundreds of atoms. Even if such charge densities are computed, the partitioning of electronic charges around each nucleus is far from trivial, especially for an iono-covalent system such as C-S-H. Here, as an alternative, we use the QEq technique[59,60] to estimate the atomic charges in C-S-H and compare them with those of the nonreactive CSHFF potential that is fitted to a database of first-principle calculations.[42] Table 1 compares the surface charge of C-S-H nanolayers from

Table 1. Surface Charge Density (SCD) of the C-S-H Nanolayer[a]

Ca/Si	1.1	1.3	1.5	1.7	1.9
relative SCD from ReaxFF (arb units)	1	0.993	0.893	0.817	0.828
relative SCD from CSHFF (arb units)	1	0.862	0.798	0.793	0.803

[a]Values are normalized with respect to 4.26 and 5.19 e/nm^2 for ReaxFF and CSHFF calculations, respectively. While both calculations follow roughly the same trend, the absolute values are different, which stems from the fixed charge assignments in CSHFF (see the Supporting Information for the charge of species).

ReaxFF and CSHFF calculations. Both calculations show almost the same trend with respect to the Ca/Si ratio; however, the absolute charge magnitudes are different. Henceforth, we use these automatically generated structures, CSHFF forcefield, and its corresponding charges for further analysis.

RESULTS AND DISCUSSION

Deviation from Continuum Description. Water molecules adjacent to C-S-H nanolayers tend to position themselves inside specific regions and form successive layers, called hydration shells.[32,33] These hydration shells are expected to influence the local permittivity of the solution and consequently the interaction between nanolayers. To further elaborate on these effects, we measure the dielectric constant of the confined water as a function of interlayer separation distance in full atomistic simulations of the interaction between C-S-H nanolayers using the CSHFF potential.

First, we place two stacked infinite C-S-H nanolayers inside a simulation box. Then, we saturate the interlayer spacing with SPC water molecules and run molecular dynamics simulation in the canonical ensemble for 8 ns; we sample the system every 10 ps in the last 5 ns. We perform this procedure for a crystalline (Ca/Si = 1.1) and glassylike (Ca/Si = 1.7) C-S-H. To examine the fidelity of calculations, we note that at large separations, the dielectric constant should converge to the bulk value and therefore can be taken as a reference data point. For bulk water, we construct a simulation box consisting of 4913 SPC rigid water molecules and run MD simulations in the isothermal−isobaric ensemble at standard condition for 5 ns while using the last 4 ns for sampling. We control pressure via the Parrinello−Rahman barostat.[61] The components of the dielectric constant can be calculated as

$$\epsilon = 1 + \beta \frac{\langle \mathbf{M}^2 \rangle - \langle \mathbf{M} \rangle^2}{3\epsilon_0 V_{\text{pore}}} \tag{3}$$

where $\mathbf{M} = \sum_{i=1}^{n} \boldsymbol{\mu}_i$, $\boldsymbol{\mu}_i$ is the dipole moment of the ith water molecule, and n is the total number of water molecules. Since the convergence of the transversal dielectric requires long simulation times, we compare the dielectric constants in the longitudinal direction (ϵ_{xy}) as the convergence can be obtained faster within a reasonable computational expense.[62]

As shown in Figure 4a, the size of the interlayer pore has a drastic effect on the dielectric constant. For smaller nanopore sizes, the dielectric constant of the medium is significantly less than that of bulk water. For large pore sizes of about 6 nm, the value of the dielectric constant calculated here is 64, which compares well with the reported value of 66.3 for rigid water molecules.[63] Overall, the strong presence of interlayer ions in glassylike C-S-H nanolayers affects the dielectric of the medium more effectively when compared with the crystalline C-S-H nanolayers. Since the variation of the Ca/Si ratio has a marginal effect on the trend of dielectric constant, we fit overall dielectric measurements with an exponentially decaying function and we find $\epsilon \propto \exp(-\zeta/\zeta_0)$, where $\zeta_0 = 13.22$ Å is the characteristic length of the decay. Based on the current results, at least 5 nm separation distance is required to procure

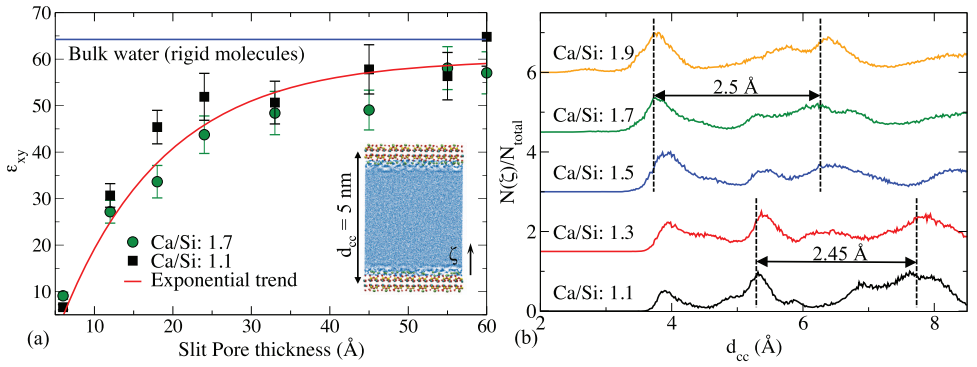

Figure 4. Presence of strong entropic effects at small nanopores. (a) Longitudinal dielectric constant versus slit pore thickness. At very short distances, the dielectric constant of the medium deviates from that of the bulk. Based on the current results, at least a 5 nm pore size is required to have a meaningful approximation of bulk water properties. The results for crystalline and glassylike C-S-H show almost identical trends. The red line shows the exponential fit to both sets of data points with $\epsilon_{xy} \propto \exp(-\zeta/13.22)$. (b) Normalized number density of oxygen atoms in water molecules adjacent to the C-S-H nanolayer. Formation of the hydration shells on the surface of the C-S-H nanolayer results in the presence of entropic hydration forces. Due to the distinction between the structures of crystalline and glassylike C-S-H, hydration shells form at various heights from the nanolayers' midplane. For the crystalline structure, the initial peak represents the existence of diffused water molecules, and later peaks depict the position of hydration shells formed on top of the nanolayers. For glassylike C-S-H, hydration shells are formed immediately on the surface. The distance between water layers is approximately 2.5 Å, which corresponds to the diameter of a rigid SPC water molecule.

DOI: 10.1021/acs.jpcc.8b08146
J. Phys. Chem. C 2019, 123, 4755−4766

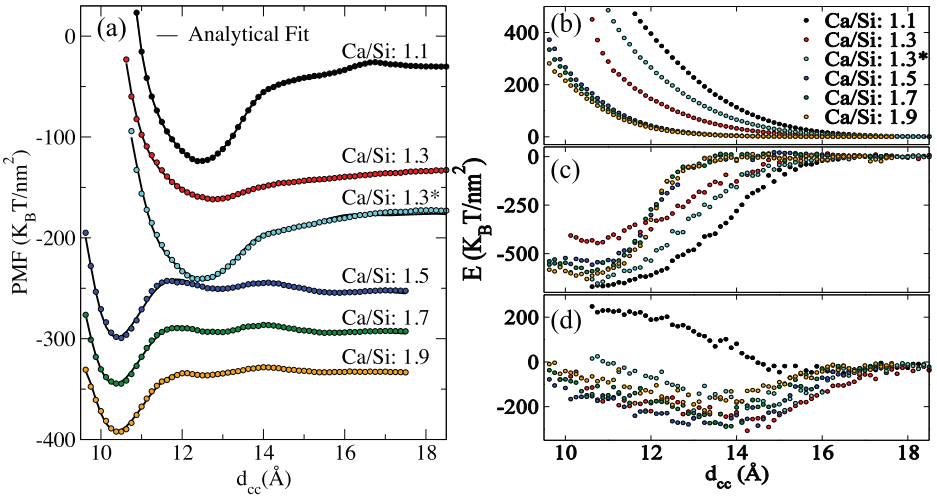

Figure 5. Interaction between C-S-H nanolayers. (a) Potential-of-mean-force (PMF) between nanolayers of C-S-H at different Ca/Si. PMFs are shifted for the sake of clarity in the representation of the graphs. For unshifted graphs, refer to the Supporting Information. For Ca/Si < 1.5, PMF graphs show a single minimum with a smooth trend, whereas the rest show multiple minima and an oscillatory trend. Also, there is a clear transition in the position of the primary minimum for glassylike structures. We associate these differences with the surface density of asperities as well as surface charge densities. Furthermore, for crystalline structures, the protocol where the increase in the Ca/Si ratio is through depolymerization of bridging sites results in a weak interaction between nanolayers of Ca/Si = 1.3. Alternatively, partial removal of bridging sites and addition of interlayer calcium atoms to increase the Ca/Si ratio to 1.3* lead to more cohesion. (b) Potential energy between two nanolayers excluding interlayer calcium hydroxyl groups (L−L). Strong repulsion arises due to the contact between nanolayers. (c) Potential energy between interlayer calcium hydroxide and the opposite nanolayer excluding its interlayer calcium hydroxide (I−L). The results portray a strong attraction between highly negative charge nanolayers of C-S-H and positively charged interlayer calcium hydroxide. (d) Potential energy between interlayer calcium hydroxide of two nanolayers (I−I). Due to the strong presence of calcium atoms and lack of hydroxyl groups, in Ca/Si = 1.1, the only repulsion arises between two groups, whereas for other Ca/Si ratios, there exist a pure attraction between nanolayers. There is also a point along the interaction path where the interaction energy is minimum. This point represents the equilibrium state of the interlayer ions inside the slit pore.

a reasonable approximation of bulk water for the hindered aqueous medium in nanopores.

Another entropic effect is the presence of hydration forces due to the formation of hydration shells around hydrophilic surfaces. In Figure 4b, we plot the normalized distribution of oxygen atoms in water molecules for different Ca/Si ratios of C-S-H nanolayers versus the center-to-center distance (d_{cc}) between nanolayers. As it appears from the graph, water molecules tend to locate in specific positions next to the C-S-H nanolayers. For crystalline C-S-H (Ca/Si < 1.5), the first peak denotes the position of diffused water molecules. The next two peaks are attributed to hydration shells formed away from C-S-H particles. For glassylike C-S-H structures (Ca/Si ≥ 1.5), water layers are formed from the position of the diffused layer of water observed for the crystalline structures. The positioning of water layers next to a crystalline and glassylike structure is dramatically affected by the spatial configuration of the surface. Also, the periodicity length of roughly 2.5 Å between shells is commensurable with the diameter of a rigid water molecule. These hydration shells are at the origins of strong entropic forces in the system, which limit the mobility of counterions and therefore cannot be simply ignored.

These results confirm that continuum theories based on distance-independent bulk properties are not accurate below 5 nm, and thus performing full atomistic simulations is critical in obtaining high-fidelity PMFs between nanolayers of C-S-H at small separation distances.

Interactions between C-S-H Nanolayers. C-S-H nanolayers predominantly interact in a face-to-face arrangement as it is the most stable form of their assembly.[16,34,39] To this end, we place two finite-sized nanolayers inside a simulation box and saturate the medium with water molecules based on the protocol explained in the Methods and Material Models section. We choose the height of the simulation box such that at the largest separation distance, there is at least 18 Å gap between nanolayers from the image cell. This is to ensure that water molecules screen interactions between nanolayers through the periodic face effectively.

Figure 5a depicts the PMF between C-S-H nanolayers for various Ca/Si. We compare the overall trend, well depth, and position of well depth in PMFs of varying Ca/Si ratios. PMFs are shifted vertically for the sake of better representation. We emphasize that the value of PMFs at the largest distance is zero for unshifted PMFs (see the Supporting Information for unshifted PMFs). As it is evident from Figure 5a, the position of well depth for Ca/Si < 1.5 is around 12.2 Å, whereas for Ca/Si ≥ 1.5, it is about 10.4 Å. To understand trends in PMF graphs, it is important to highlight differences between surface density of asperities in the crystalline and glassylike structures of C-S-H developed in this work. At Ca/Si < 1.5, bridging sites protruding from the nanolayer cause an early contact with the opposite nanolayer in comparison to C-S-H nanolayers where no bridging site is present. Based on the protocol explained in the preparation of atomic structure of C-S-H in this work, for Ca/Si < 1.5, the number of bridging sites reduces as the Ca/Si ratio increases and becomes zero at Ca/Si = 1.5. As long as they exist on the surface, regardless of their density, protruding sites cause early contact at the same level. In other words, the number of protruding sites determines the intensity of repulsive forces before contact, but the contact itself is the extreme case and it will cause a strong repulsion even for a single contact point. This explains the transition in the position of well depth in our models. In addition, PMF for Ca/Si = 1.3 shows a significantly weak interaction, which is rather

DOI: 10.1021/acs.jpcc.8b08146
J. Phys. Chem. C 2019, 123, 4755−4766

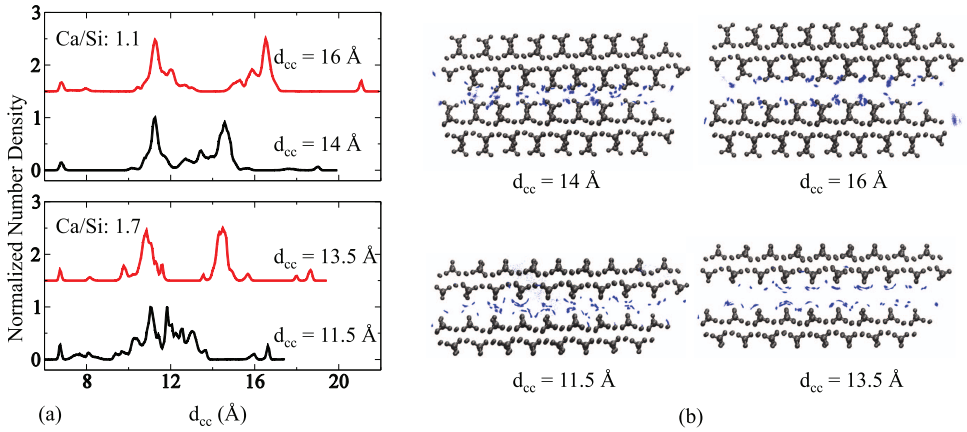

Figure 6. Distribution of interlayer calcium atoms inside the slit nanopore. (a) Normalized number density of interlayer calcium atoms at different center-to-center distances for a crystalline and glassylike C-S-H. Interlayer calcium atoms are more mobile adjacent to a glassylike C-S-H nanolayer, whereas they are strongly bonded to their corresponding nanolayer next to a crystalline structure. The increase in center-to-center distance results in easier separation of interlayer calcium atoms from the nanolayer surface. (b) Trajectory of the position of interlayer calcium atoms in the last 500 ps of the MD simulations shown as blue dots. Interlayer calcium atoms can explore bigger regions during their vibrations adjacent to a glassylike C-S-H structure when compared to a crystalline C-S-H structure.

unexpected. This stems from weaker SCD at the level of bridging sites as a result of a smaller number of bridging sites. To study the impact of polymorphism on intermolecular forces, we construct a C-S-H structure by increasing the Ca/Si ratio based on depolymerization of silicates and adding interlayer calcium, and we find an SCD of 6.1 e/nm^2. For simplicity, we denote this sample by Ca/Si = 1.3*. We observe that the trend for Ca/Si = 1.3* exhibits a more realistic PMF. This implies that the increase in Ca/Si at the crystalline phase of the C-S-H cannot be only due to the removal of bridging sites as such structures are weakly bonded. The weak bond between crystalline C-S-H nanolayers has never been reported experimentally, and it is rather implausible. For glassylike C-S-H, the position of well depth remains almost the same at around 10.4 Å regardless of Ca/Si, emphasizing the dominant role of the surface morphology on the equilibrium distance. For Ca/Si $\geq$ 1.5, removing dimers and replacing them with hydroxyl groups leaves a negative charge in the nanolayer, causing larger well depth. However, the energy barrier, which is the difference between the primary minimum and subsequent maximum, remains almost the same. The presence of repulsive interactions for glassylike C-S-H is due to the double-layer entropic forces along with ionic fluctuations.[22] Also, the existence of the hydration shells adjacent to the C-S-H nanolayer leads to the presence of hydration forces in the system and subsequently an oscillatory behavior in PMFs. The oscillatory trend is more conspicuous for glassylike C-S-H. This is significant as the observed trends resemble what the conventional DLVO theory usually predicts. However, the contributing forces are fundamentally different due to their local nature.

To gain a more comprehensive insight into the interactions between nanolayers of C-S-H, we conduct a series of detailed studies on nonbond interactions between a group of atoms in the first nanolayer and a group of atoms in the second nanolayer. For simplicity, we call the nanolayer without the interlayer ions (interlayer calcium atoms and hydroxyl groups) "L" and with the interlayer ions "I". Figure 5b shows the L−L interaction. The difference between trends of L−L interaction for Ca/Si = 1.1 and Ca/Si = 1.3 is mainly due to the number density of bridging sites. This is because the greater the contact area is, the more intense the repulsion becomes. This further demonstrates that the contact between protruding sites dominates the repulsion at very short distances. For Ca/Si = 1.3*, there are more bridging sites on the surface than Ca/Si = 1.3, and as a result, the repulsion at contact is more notable. It is interesting to note that all crystalline structures, regardless of the Ca/Si ratio, would have exceedingly large repulsion at the same distance due to the contacts between bridging sites. For Ca/Si > 1.5, where no bridging site is available in our current models, hard contact extends to larger penetrations comparable to the size of bridging sites.

The I−I interaction, depicted in Figure 5c, in a nutshell, is the interplay between similar charges repelling each other and opposite charges attracting one another. For Ca/Si = 1.1, the repulsion between calcium atoms dominates the overall interaction. The concentration of anions at the surface of the C-S-H nanolayer rises with the increase in the Ca/Si ratio. For Ca/Si = 1.3 and Ca/Si = 1.3*, the presence of more hydroxyl groups increases the total attraction between calcium atoms and hydroxyl groups. Nevertheless, for Ca/Si = 1.3*, adding more calcium atoms induces more repulsion, which in fact dominates the total I−I interaction (see the Supporting Information for detailed interactions between interlayer calcium−calcium, interlayer calcium-hydroxyl, and hydroxyl−hydroxyl). For the case of Ca/Si = 1.5, the interaction strengthens as the number of hydroxyl groups in interlayer Ca−OH is at its peak. For larger Ca/Si, removing dimers from the nanolayer causes protons to diffuse into the nanolayer and form hydroxyl groups and then position next to the central calcium sheet, forming intralayer CaOH (see Figure 3). Hence, these hydroxyl groups are farther from the counterions of the opposite nanolayer and have a minimal effect on the attraction between total calcium atoms and hydroxyl groups (see the Supporting Information). Another noteworthy feature is that I−I interactions show a minimum across the pore thickness. This minimum accentuates the distance in which ions interact in their equilibrium states due to the adequate volume available. This finding indicates that the equilibrium distance between nanolayers does not guarantee the equilibrium between interlayer ions.

DOI: 10.1021/acs.jpcc.8b08146
J. Phys. Chem. C 2019, 123, 4755−4766

Table 2. Constants of the Proposed Analytical PMF Formula in Equation 4 for C-S-H Nanolayers with Varying Ca/Si Ratios

Ca/Si	a_1 (K_BT/nm^2)	b_1	c_1	d_1	a_2 (Å)	b_2 (Å)	c_2 (Å)	d_2 (Å)	d_3(Å)
1.1	8769	0.879	0.962	0.0054	1.00	0.71	5.83	2.49	0.87
1.3	7198	1.186	1.035	0.0068	0.79	0.69	5.74	2.48	0.84
1.3*	5399	0.88	0.83	0.0051	1.00	0.73	6.34	2.41	0.80
1.5	999	0.978	2.280	0.026	0.93	0.41	3.19	2.55	0.98
1.7	906	0.734	1.892	0.024	1.05	0.41	3.45	2.46	0.85
1.9	734	1.183	1.887	0.024	0.84	0.40	3.59	2.4	0.73

Table 3. Comparison between Mechanical Properties of C-S-H Nanolayers Calculated from PMFs in this Work and Experimental Measurements from the Literature

	Ca/Si						
property	1.1	1.3	1.3*	1.5	1.7	1.9	experiments
E (GPa)	73.56	26.15	52.3	102.43	81.74	89.58	61,[65] 89,[67] >88.9[64]
γ_s (J/m^2)	0.3473	0.1065	0.2511	0.1716	0.1905	0.2189	0.1,[70] 0.32−0.4[68,69]
P_{co} (GPa)	2.9	0.9	1.9	3.7	3	3.1	5,[34,73] 0.93[74]

The interaction between the nanolayer and ions at the surface of the opposite nanolayer plays an important role in the total interaction. The negatively charged nanolayer of C-S-H is attracted by the interlayer calcium atoms and a minor repulsion from hydroxyl groups of the other side. The combined effect of these forces determines the overall interaction. Figure 5d depicts the total interaction between L−I. As illustrated in the figure, the attraction between interlayer calcium atoms and the opposite nanolayer outweighs the repulsion between the nanolayer and hydroxyl groups. In addition, crystalline nanolayers are thicker than glassylike nanolayers, and consequently the range in which L−I interaction is active would be longer. The interaction for crystalline nanolayers shows gradual retardation, whereas for glassylike nanolayers it exhibits a sharp change. In the limit of very short distances, the confinement enforces the counterions to reabsorb onto the surface sites and become part of the nanolayer, which prompts slower dynamics of interlayer calcium atoms as well as reduction of apparent surface charge.[22] Pushing the nanolayers further causes the counterions and nanolayer to come into contact, and this will provoke a strong repulsion in the interaction.

We depict the distribution of interlayer calcium atoms in the nanopore in Figure 6 to analyze their mobility around a crystalline (Ca/Si = 1.1) and glassylike (Ca/Si = 1.7) C-S-H nanolayer at different d_{cc}. For a crystalline structure (Ca/Si = 1.1), peaks are sharper and located at the surface of the C-S-H nanolayer at different d_{cc}. At closer distances, due to the strong attraction from the other nanolayers, interlayer calcium atoms tend to position closer to the midplane. For the glassylike structure, peaks are wider, indicating more mobility. This is more pronounced when nanolayers are closer and the distribution is wider in the interlayer pore. Figure 6b illustrates the trajectory of interlayer calcium atoms during the last 500 ps of the MD simulations sampled every 2 ps corresponding to 250 points for each atom. As it is evident from the trajectory map, interlayer calcium atoms show higher mobility for the glassylike structure, indicating less repulsion from the opposite counterions. This is vividly reflected in the interaction between interlayer calcium atoms shown in the Supporting Information.

To explain the interaction between C-S-H nanolayers, we seek a versatile analytical model that can fit our FEP results. Here, we consider four different contributions to the total PMF. First, the effect of van der Waals interaction needs to be taken into account. Although the surface of C-S-H is not flat, for simplicity we use $E_{vdW} \propto d_{cc}^{-2}$ for flat surfaces.[22] Another important term in the total interaction is the contact between nanolayers, which we take it as a soft contact and represent it via $E_{steric\text{-}contact} \propto \exp(-d_{cc})$. To capture the electrostatic interaction, we use screened Coulomb potential as $E_{Yukawa} \propto \exp(-d_{cc})/d_{cc}$. Furthermore, we consider the effects of hydration forces and liquid layering at short separations via $E_{hyd} \propto \exp(-d_{cc})\sin(d_{cc})$.[22,34] In total, the PMF per unit area between nanolayers of C-S-H can be expressed as

$$A^{rel} = a_1\left(-\frac{1}{(\bar{x}+a_2)^2} + b_1\exp\left(-\frac{\bar{x}}{b_2}\right) + c_1\frac{\exp\left(-\frac{\bar{x}}{c_2}\right)}{\bar{x}+h} + d_1\exp\left(-\frac{\bar{x}}{d_2}\right)\sin\left(\frac{2\pi(\bar{x}+d_3)}{d_2}\right)\right) \quad (4)$$

where $\bar{x} = d_{cc} - 9.5$ is the transformed coordinate. a_1 and a_2 are, respectively, the strength and shifting distance to the infinite attractive energies. b_1 and b_2 are, respectively, the relative strength and characteristic length of decay for steric contact energies. c_1 and c_2 are the relative strength and characteristic length of decay in the Yukawa potential, respectively, whereas h is the effective thickness of nanolayers where for crystalline and glassylike structures they are 11.5 and 9.5 Å, respectively. In addition, d_1, d_2, and d_3 are the relative strength, periodicity length of the hydration force, and phase of the Sine wave, respectively. Figure 5a depicts the analytical PMF fits with an excellent match with FEP results. The value of coefficients after the fitting exercise is given in Table 2. The normalized values clearly indicate a significant increase in the contribution of the Yukawa term corresponding to the screened Coulomb potential for glassylike C-S-H structures compared to crystalline C-S-H structures. Another notable difference between the hydration interaction energy in glassylike and crystalline structures is that the latter is approximately 4 times greater than the former. From the analytical potential function, we can clearly observe that the existence of immediate maximum after primary minimum as well as oscillations in PMFs of glassylike structures can be only attributed to the presence of screened coulomb potential and hydration forces.

DOI: 10.1021/acs.jpcc.8b08146
J. Phys. Chem. C 2019, 123, 4755−4766

Mechanical Properties of C-S-H at the Nanoscale. Access to the PMF provides information about some of the key parameters such as elastic modulus, interfacial energy, and cohesive pressure at the molecular level. Here, we calculate elastic modulus from PMF as

$$E_{zz} = d_0\left(\frac{\partial^2\langle A^{rel}\rangle}{\partial\zeta^2}\right)_{d_0} \quad (5)$$

where d_0 is the position of well depth in PMF. Also, we compute interfacial energy as

$$\gamma_s = \left(-\frac{\langle A^{rel}\rangle}{2}\right)_{d_0} \quad (6)$$

Table 3 shows these values for different Ca/Si ratios. Our results show a slight increase in the elastic modulus. Increase in the elastic modulus has also been reported for the case of increasing calcium concentration in the solution, which can be interpreted as the increase in the Ca/Si ratio.[64] This marks the prominence of spatial configurations while dealing with particles' interaction. We compare our result with available experimental measurements. We find a good agreement between the range of variations in computed elastic modulus and atomic force microscope measurements of 88.9 GPa (and greater values for more calcium concentration)[64] and high-pressure X-ray diffraction values of 61[65,66] and 89[67] for C-S-H(I) and 14 Å Tobermorite, respectively. Our computed interfacial energy is within the range of 0.1−0.35 J/m^2, comparable with the experimental report for the Tobermorite structure[68,69] and the value of 0.1 J/m^2 reported for C-S-H(I)[70] as well as fracture surface energy calculations.[71,72] Moreover, we calculate the cohesive pressure (maximum mean force per area) for our C-S-H models in relative humidity = 100%, and we find the maximum value of 3.7 GPa for Ca/Si = 1.5. The results available for comparison are 5 GPa, worked out via molecular dynamics simulation for the Tobermorite structure,[34,73] and 0.93 GPa for C-S-H with Ca/Si = 1.65 and relative humidity of 10%[39] as well as experimental result of 0.93 GPa for C-S-H with Ca/Si 1.7 in dry air condition. We emphasize that our simulation results are in molecular level, and therefore higher mechanical properties than experimental measurements are expected as the presence of porosity and defects at the higher scales cannot be included in molecular-level simulations. Taking into account this fact, our results are in good agreement with experimental results.

CONCLUSIONS

In this paper, we report a molecular-level study on the effective interaction between C-S-H nanolayers with corrugated surfaces using the FEP method. We summarize our key points as follows:

- When considering interactions between particles at the nanoscale and within short distances, local effects such as surface density of asperities and formation of hydration shells play a dominant role. As such, any calculations in this regard should address these effects.
- For a finite-sized C-S-H nanolayer, reactive simulations show a full protonation of ending sites to balance the charge of silicate tetrahedra.
- Full atomistic simulations reveal that at least 5 nm separation distance between nanoparticles is required when considering dielectric continuum assumption. The dielectric constant shows an exponentially decaying correlation with respect to the separation distance $\epsilon \propto \exp\left(\frac{-\zeta}{\eta}\right)$, where η is the characteristic length of the decay. For C-S-H nanolayers studied in this work, we find η = 13.2 Å.
- The total CaOH content in C-S-H can be divided into the contribution of the interlayer and intralayer calcium atoms. The former is present at all Ca/Si ratios, and its contribution becomes constant as the latter emerge at Ca/Si $\geq$ 1.5. The total CaOH/Si ratio increases proportionally with the rise of the Ca/Si ratio from 1.1 to 1.9 in accordance with INS measurements.[57]
- In addition to the electrostatic interactions between particles, the spatial configuration of the surface determines the strength of interactions at short distances. There is a clear transition in the PMF trend from a crystalline structure to the glassylike structure of C-S-H nanolayers. The presence of hydration forces and complete removal of protruding silicate tetrahedra dictates a DLVO-like trend at short distances. However, the source of the repulsion forces is completely different and needs to be discussed with reference to the local effects. From interaction analysis, we find that removal of bridging silicate tetrahedra affects the range of interactions accordingly. This further proves the complex influence of surface morphology on the PMF.
- A mere removal of silicon atoms to achieve a higher Ca/Si ratio during the structural transition from the crystalline to the glassylike C-S-H structure (when only a few bridging sites are available) results in a weak cohesion and mechanical properties. For the sake of modeling C-S-H nanolayers, it is more realistic to consider the simultaneous addition of interlayer calcium atoms and removal of silicon atoms to increase Ca/Si during the transition from crystalline to the glassylike structure.
- Interlayer calcium atoms are less bounded to the nanolayers of C-S-H at larger Ca/Si ratios. This is related to the lower surface asperity density. Also, at larger separation distances, due to the increase in availability of interlayer space, the induced pressure from the interplay between counterions of opposing nanolayers decreases. This allows counterions to move farther away from the nanolayers without encountering strong repulsion from the opposite layer.

The current paper attempts to fill the gap between nano- and mesoscale modeling by providing the key thermodynamic upscaling quantity, that is, the potential-of-mean-force. Contrary to the conventional mean-field theories, the proposed potential is derived from full atomistic simulations and considers the entropic effects between C-S-H nanoparticles. Therefore, we expect that our proposed PMFs facilitate a systematic mesotextural,[4−6] mechanical,[75] and thermal[76,77] investigation of cementitious materials at the mesoscale.

ASSOCIATED CONTENT

Supporting Information

The Supporting Information is available free of charge on the ACS Publications website at DOI: 10.1021/acs.jpcc.8b08146.

DOI: 10.1021/acs.jpcc.8b08146
J. Phys. Chem. C 2019, 123, 4755−4766

Reaction between oxygen atoms in C-S-H layers and the aqueous solution, charge of species, unshifted PMFs between nanolayers of C-S-H, interaction potential energy between interlayer atoms, and finite-sized boundary condition (PDF)

AUTHOR INFORMATION

Corresponding Author

*E-mail: mjaq@uci.edu.

ORCID

Mohammad Javad Abdolhosseini Qomi: 0000-0001-6911-0994

Notes

The authors declare no competing financial interest.

ACKNOWLEDGMENTS

We would like to acknowledge fruitful discussions with Drs Davoud Ebrahimi and Konrad Krakowiak. This work was supported in part by the National Science Foundation under Award No. CMMI-1826122. Any opinions, findings, and conclusions or recommendations expressed in this material are those of the authors and do not necessarily reflect those of the National Science Foundation. Computational resources used in this work were provided by Intersect Australia Ltd, the National Computational Infrastructure (NCI), which is supported by the Australian Government, high-performance computing centers at UNSW Sydney and University of California Irvine.

REFERENCES

(1) Rahimi-Aghdam, S.; Bažant, Z. P.; Abdolhosseini Qomi, M. J. Cement hydration from hours to centuries controlled by diffusion through barrier shells of C-S-H. *J. Mech. Phys. Solids* **2017**, *99*, 211−224.

(2) Ioannidou, K.; Pellenq, R. J.-M.; Gado, E. D. Controlling local packing and growth in calcium-silicate-hydrate gels. *Soft Matter* **2014**, *10*, 1121−1133.

(3) Ioannidou, K.; Kanduč, M.; Li, L.; Frenkel, D.; Dobnikar, J.; Gado, E. D. The crucial effect of early-stage gelation on the mechanical properties of cement hydrates. *Nat. Commun.* **2016**, *7*, No. 12106.

(4) Shvab, I.; Brochard, L.; Manzano, H.; Masoero, E. Precipitation Mechanisms of Mesoporous Nanoparticle Aggregates: Off-Lattice, Coarse-Grained, Kinetic Simulations. *Cryst. Growth Des.* **2017**, *17*, 1316−1327.

(5) Ioannidou, K.; Krakowiak, K. J.; Bauchy, M.; Hoover, C. G.; Masoero, E.; Yip, S.; Ulm, F.-J.; Levitz, P.; Pellenq, R. J.-M.; Gado, E. D. Mesoscale texture of cement hydrates. *Proc. Natl. Acad. Sci. U.S.A.* **2016**, *113*, 2029−2034.

(6) Masoero, E.; Gado, E. D.; Pellenq, R. J.-M.; Yip, S.; Ulm, F.-J. Nano-scale mechanics of colloidal C-S-H gels. *Soft Matter* **2014**, *10*, 491−499.

(7) Pellenq, R. J.-M.; Kushima, A.; Shahsavari, R.; Vliet, K. J. V.; Buehler, M. J.; Yip, S.; Ulm, F.-J. a realistic molecular model of cement hydrates. *Proc. Natl. Acad. Sci. U.S.A.* **2009**, *106*, 16102−16107.

(8) Qomi, M. A.; Krakowiak, K. J.; Bauchy, M.; Stewart, K. L.; Shahsavari, R.; Jagannathan, D.; Brommer, D. B.; Baronnet, A.; Buehler, M. J.; Yip, S. Combinatorial molecular optimization of cement hydrates. *Nat. Commun.* **2014**, *5*, No. 4960.

(9) Richardson, I. G. the calcium silicate hydrates. *Cem. Concr. Res.* **2008**, *38*, 137−158.

(10) Gartner, E.; Maruyama, I.; Chen, J. A new model for the C-S-H phase formed during the hydration of Portland cements. *Cem. Concr. Res.* **2017**, *97*, 95−106.

(11) Kovačević, G.; Persson, B.; Nicoleau, L.; Nonat, A.; Veryazov, V. Atomistic modeling of crystal structure of Ca1.67SiHx. *Cem. Concr. Res.* **2015**, *67*, 197−203.

(12) Taylor, H. F. Proposed Structure for Calcium Silicate Hydrate Gel. *J. Am. Ceram. Soc.* **1986**, *69*, 464−467.

(13) Jennings, H. M. Refinements to colloid model of C-S-H in cement: CM-II. *Cem. Concr. Res.* **2008**, *38*, 275−289.

(14) Constantinides, G.; Ulm, F. J. the effect of two types of C-S-H on the elasticity of cement-based materials: Results from nano-indentation and micromechanical modeling. *Cem. Concr. Res.* **2004**, *34*, 67−80.

(15) Allen, A. J.; Oberthur, R. C.; Pearson, D.; Schofield, P.; Wilding, C. R. Development of the fine porosity and gel structure of hydrating cement systems. *Philos. Mag. B* **1987**, *56*, 263−288.

(16) Chiang, W.-S.; Fratini, E.; Baglioni, P.; Liu, D.; Chen, S.-H. Microstructure Determination of Calcium-Silicate-Hydrate Globules by Small-Angle Neutron Scattering. *J. Phys. Chem. C* **2012**, *116*, 5055−5061.

(17) Chiang, W.-S.; Ferraro, G.; Fratini, E.; Ridi, F.; Yeh, Y.-Q.; Jeng, U.-S.; Chen, S.-H.; Baglioni, P. Multiscale structure of calcium- and magnesium-silicate-hydrate gels. *J. Mater. Chem. A* **2014**, *2*, 12991−12998.

(18) Grangeon, S.; Claret, F.; Roosz, C.; Sato, T.; Gaboreau, S.; Linard, Y. Structure of nanocrystalline calcium silicate hydrates: insights from X-ray diffraction, synchrotron X-ray absorption and nuclear magnetic resonance. *J. Appl. Crystallogr.* **2016**, *49*, 771−783.

(19) Krakowiak, K. J.; Thomas, J. J.; James, S.; Abuhaikal, M.; Ulm, F. J. Development of silica-enriched cement-based materials with improved aging resistance for application in high-temperature environments. *Cem. Concr. Res.* **2018**, *105*, 91−110.

(20) Geng, G.; Vasin, R. N.; Li, J.; Qomi, M. J. A.; Yan, J.; Wenk, H.-R.; Monteiro, P. J. M. Preferred orientation of calcium aluminosilicate hydrate induced by confined compression. *Cem. Concr. Res.* **2018**, *113*, 186−196.

(21) Pellenq, R. J.-M.; Caillol, J. M.; Delville, A. Electrostatic Attraction between Two Charged Surfaces: A (N,V,T) Monte Carlo Simulation. *J. Phys. Chem. B* **1997**, *101*, 8584−8594.

(22) Israelachvili, J. N. *Intermolecular and Surface Forces: Revised Third Edition*; Academic Press: Cambridge, MA, 2011.

(23) Patey, G. N. The interaction of two spherical colloidal particles in electrolyte solution. An application of the hypernetted chain approximation. *J. Chem. Phys.* **1980**, *72*, 5763−5771.

(24) Belloni, L. Colloidal interactions. *J. Phys.: Condens. Matter* **2000**, *12*, No. R549.

(25) Tavares, F. W.; Bratko, D.; Blanch, H. W.; Prausnitz, J. M. Ion-Specific Effects in the Colloid-Colloid or Protein-Protein Potential of Mean Force: Role of Salt-Macroion van der Waals Interactions. *J. Phys. Chem. B* **2004**, *108*, 9228−9235.

(26) Bhattacharjee, S.; Ko, C.-H.; Elimelech, M. DLVO Interaction between Rough Surfaces. *Langmuir* **1998**, *14*, 3365−3375.

(27) Christenson, H. K. Non-Dlvo Forces Between Surfaces -Solvation, Hydration and Capillary Effects. *J. Dispersion Sci. Technol.* **1988**, *9*, 171−206.

(28) Derjaguin, B.; Landau, L. Theory of the stability of strongly charged lyophobic sols and of the adhesion of strongly charged particles in solutions of electrolytes. *Acta Physicochim. URSS* **1941**, *14*, 633−662.

(29) Verwey, E. J. W.; Overbeek, J. T. G. *Theory of the Stability of Lyophobic Colloids*; Courier Corporation: NY, 1999.

(30) Jönsson, B.; Nonat, A.; Labbez, C.; Cabane, B.; Wennerström, H. Controlling the Cohesion of Cement Paste. *Langmuir* **2005**, *21*, 9211−9221.

(31) Jönsson, B.; Wennerström, H.; Nonat, A.; Cabane, B. Onset of Cohesion in Cement Paste. *Langmuir* **2004**, *20*, 6702−6709.

(32) Masoumi, S.; Valipour, H.; Abdolhosseini Qomi, M. J. Intermolecular Forces between Nanolayers of Crystalline Calcium-Silicate-Hydrates in Aqueous Medium. *J. Phys. Chem. C* **2017**, *121*, 5565−5572.

DOI: 10.1021/acs.jpcc.8b08146
J. Phys. Chem. C 2019, 123, 4755−4766

(33) Kalinichev, A. G.; Wang, J.; Kirkpatrick, R. J. Molecular dynamics modeling of the structure, dynamics and energetics of mineral-water interfaces: Application to cement materials. *Cem. Concr. Res.* **2007**, *37*, 337−347.
(34) Masoumi, S.; Valipour, H.; Abdolhosseini Qomi, M. J. Interparticle Interactions in Colloidal Systems: Toward a Comprehensive Mesoscale Model. *ACS Appl. Mater. Interfaces* **2017**, *9*, 27338−27349.
(35) Viallis-Terrisse, H.; Nonat, A.; Petit, J.-C. ζ-Potential Study of Calcium Silicate Hydrates Interacting with Alkaline Cations. *J. Colloid Interface Sci.* **2001**, *244*, 58−65.
(36) Qomi, M. J. A.; Bauchy, M.; Ulm, F.-J.; Pellenq, R. J.-M. anomalous composition-dependent dynamics of nanoconfined water in the interlayer of disordered calcium-silicates. *J. Chem. Phys.* **2014**, *140*, No. 054515.
(37) Ebrahimi, D.; Pellenq, R. J.-M.; Whittle, A. J. nanoscale elastic properties of montmorillonite upon water adsorption. *Langmuir* **2012**, *28*, 16855−16863.
(38) Ebrahimi, D.; Whittle, A. J.; Pellenq, R. J.-M. Mesoscale properties of clay aggregates from potential of mean force representation of interactions between nanoplatelets. *J. Chem. Phys.* **2014**, *140*, No. 154309.
(39) Bonnaud, P. A.; Labbez, C.; Miura, R.; Suzuki, A.; Miyamoto, N.; Hatakeyama, N.; Miyamoto, A.; Vliet, K. J. V. Interaction grand potential between calcium-silicate-hydrate nanoparticles at the molecular level. *Nanoscale* **2016**, *8*, 4160−4172.
(40) Plimpton, S. Fast parallel algorithms for short-range molecular dynamics. *J. Comput. Phys.* **1995**, *117*, 1−19.
(41) Shahsavari, R.; Buehler, M. J.; Pellenq, R. J.-M.; Ulm, F.-J. first-principles study of elastic constants and interlayer interactions of complex hydrated oxides: case study of tobermorite and jennite. *J. Am. Ceram. Soc.* **2009**, *92*, 2323−2330.
(42) Shahsavari, R.; Pellenq, R. J.-M.; Ulm, F.-J. empirical force fields for complex hydrated calcio-silicate layered materials. *Phys. Chem. Chem. Phys.* **2011**, *13*, 1002−1011.
(43) Bonnaud, P. A.; Ji, Q.; Vliet, K. J. V. Effects of elevated temperature on the structure and properties of calcium-silicate-hydrate gels: the role of confined water. *Soft Matter* **2013**, *9*, 6418−6429.
(44) Qomi, M. J. A.; Bauchy, M.; Ulm, F.-J.; Pellenq, R. In *Nanotechnology in Construction*; Sobolev, K., Shah, S. P., Eds.; Springer International Publishing, 2015; pp 99−108.
(45) Martyna, G. J.; Klein, M. L.; Tuckerman, M. Nosé-Hoover chains: The canonical ensemble via continuous dynamics. *J. Chem. Phys.* **1992**, *97*, 2635−2643.
(46) Chipot, C.; Pohorille, A. *Free Energy Calculations*; Springer-Verlag: Berlin, Heidelberg, 2007.
(47) Hamid, S. the crystal-structure of the 11A natural tobermorite Ca2.25[Si3O7.5(OH)1.5].1H2O. *Z. Kristallogr. - Cryst. Mater.* **1981**, *154*, 189−198.
(48) Megaw, H. D.; Kelsey, C. H. Crystal Structure of Tobermorite. *Nature* **1956**, *177*, 390−391.
(49) Chen, J. J.; Thomas, J. J.; Taylor, H. F.; Jennings, H. M. solubility and structure of calcium silicate hydrate. *Cem. Concr. Res.* **2004**, *34*, 1499−1519.
(50) Cong, X.; Kirkpatrick, R. 29Si MAS NMR study of the structure of calcium silicate hydrate. *Adv. Cem. Based Mater.* **1996**, *3*, 144−156.
(51) Haas, R.; Biermayr, P. The rebound effect for space heating Empirical evidence from Austria. *Energy Policy* **2000**, *28*, 403−410.
(52) Yu, P.; Kirkpatrick, R. J.; Poe, B.; McMillan, P. F.; Cong, X. Structure of Calcium Silicate Hydrate (C-S-H): Near-, Mid-, and Far-Infrared Spectroscopy. *J. Am. Ceram. Soc.* **1999**, *82*, 742−748.
(53) Nonat, A. The structure and stoichiometry of C-S-H. *Cem. Concr. Res.* **2004**, *34*, 1521−1528.
(54) Chenoweth, K.; van Duin, A. C. T.; Goddard, W. A. ReaxFF Reactive Force Field for Molecular Dynamics Simulations of Hydrocarbon Oxidation. *J. Phys. Chem. A* **2008**, *112*, 1040−1053.
(55) Manzano, H.; Moeini, S.; Marinelli, F.; van Duin, A. C. T.; Ulm, F.-J.; Pellenq, R. J.-M. confined water dissociation in microporous defective silicates: mechanism, dipole distribution, and impact on substrate properties. *J. Am. Chem. Soc.* **2012**, *134*, 2208−2215.
(56) Manzano, H.; Pellenq, R. J. M.; Ulm, F.-J.; Buehler, M. J.; van Duin, A. C. T. hydration of calcium oxide surface predicted by reactive force field molecular dynamics. *Langmuir* **2012**, *28*, 4187−4197.
(57) Thomas, J. J.; Chen, J. J.; Jennings, H. M.; Neumann, D. A. Ca−OH bonding in the C-S-H gel phase of tricalcium silicate and white portland cement pastes measured by inelastic neutron scattering. *Chem. Mater.* **2003**, *15*, 3813−3817.
(58) Richardson, I. G. the nature of the hydration products in hardened cement pastes. *Cem. Concr. Compos.* **2000**, *22*, 97−113.
(59) Nakano, A. Parallel multilevel preconditioned conjugate-gradient approach to variable-charge molecular dynamics. *Comput. Phys. Commun.* **1997**, *104*, 59−69.
(60) Rappe, A. K.; Goddard, W. A. Charge equilibration for molecular dynamics simulations. *J. Phys. Chem.* **1991**, *95*, 3358−3363.
(61) Parrinello, M.; Rahman, A. Polymorphic transitions in single crystals: A new molecular dynamics method. *J. Appl. Phys.* **1981**, *52*, 7182−7190.
(62) Carrier, B. Influence of Water on the Short-term and Long-term Mechanical Properties of Swelling Clays: Experiments on Self-Supporting Films and Molecular Simulations. Ph.D. Thesis, Université Paris-Est, 2013.
(63) Wu, Y.; Tepper, H. L.; Voth, G. A. Flexible simple point-charge water model with improved liquid-state properties. *J. Chem. Phys.* **2006**, *124*, No. 024503.
(64) Plassard, C.; Lesniewska, E.; Pochard, I.; Nonat, A. Investigation of the surface structure and elastic properties of calcium silicate hydrates at the nanoscale. *Ultramicroscopy* **2004**, *100*, 331−338.
(65) Oh, J. E.; Clark, S. M.; Monteiro, P. J. M. Does the Al substitution in C-S-H(I) change its mechanical property? *Cem. Concr. Res.* **2011**, *41*, 102−106.
(66) Geng, G.; Myers, R. J.; Qomi, M. J. A.; Monteiro, P. J. M. Densification of the interlayer spacing governs the nanomechanical properties of calcium-silicate-hydrate. *Sci. Rep.* **2017**, *7*, No. 10986.
(67) Oh, J. E.; Clark, S. M.; Wenk, H.-R.; Monteiro, P. J. M. Experimental determination of bulk modulus of 14 Å tobermorite using high pressure synchrotron X-ray diffraction. *Cem. Concr. Res.* **2012**, *42*, 397−403.
(68) Brunauer, S.; Kantro, D. L.; Weise, C. H. The Surface Energy of Tobermorite. *Can. J. Chem.* **1959**, *37*, 714−724.
(69) Brunauer, S. Surfaces of solids. *Pure Appl. Chem.* **1965**, *10*, 293−308.
(70) Bullard, J. W.; Scherer, G. W.; Thomas, J. J. Time dependent driving forces and the kinetics of tricalcium silicate hydration. *Cem. Concr. Res.* **2015**, *74*, 26−34.
(71) Bauchy, M.; Laubie, H.; Abdolhosseini Qomi, M. J.; Hoover, C. G.; Ulm, F. J.; Pellenq, R. J. M. Fracture toughness of calcium-silicate-hydrate from molecular dynamics simulations. *J. Non-Cryst. Solids* **2015**, *419*, 58−64.
(72) Bauchy, M.; Wang, B.; Wang, M.; Yu, Y.; Abdolhosseini Qomi, M. J.; Smedskjaer, M. M.; Bichara, C.; Ulm, F.-J.; Pellenq, R. Fracture toughness anomalies: Viewpoint of topological constraint theory. *Acta Mater.* **2016**, *121*, 234−239.
(73) Pellenq, R. J. M.; Lequeux, N.; van Damme, H. Engineering the bonding scheme in C-S-H: The iono-covalent framework. *Cem. Concr. Res.* **2008**, *38*, 159−174.
(74) Plassard, C.; Lesniewska, E.; Pochard, I.; Nonat, A. Nanoscale Experimental Investigation of Particle Interactions at the Origin of the Cohesion of Cement. *Langmuir* **2005**, *21*, 7263−7270.
(75) Morshedifard, A.; Masoumi, S.; Qomi, M. J. A. Nanoscale origins of creep in calcium silicate hydrates. *Nat. Commun.* **2018**, *9*, No. 1785.
(76) Qomi, M. J. A.; Ulm, F.-J.; Pellenq, R. J.-M. Physical origins of thermal properties of cement paste. *Phys. Rev. Appl.* **2015**, *3*, No. 064010.

DOI: 10.1021/acs.jpcc.8b08146
J. Phys. Chem. C 2019, 123, 4755−4766

(77) Zhou, Y.; Morshedifard, A.; Lee, J.; Abdolhosseini Qomi, M. J. The contribution of propagons and diffusons in heat transport through calcium-silicate-hydrates. *Appl. Phys. Lett.* **2017**, *110*, No. 043104.

DOI: 10.1021/acs.jpcc.8b08146
J. Phys. Chem. C 2019, 123, 4755−4766